CHAPTER 5

Salinity Gradient Energy

Kitty Nijmeijer[1,*] *and* **Sybrand Metz**[2]
[1]Membrane Technology Group, Institute of Mechanics, Processes and Control Twente (IMPACT), University of Twente, P.O. Box 217, 7500 AE Enschede, The Netherlands
[2]Wetsus, Centre of Excellence for Sustainable Water Technology, P.O. Box 1113, 8900 CC Leeuwarden, The Netherlands

Contents

1. INTRODUCTION

Since the Kyoto protocol and the report of the Intergovernmental Panel on Climate Change (IPCC) [1] on carbon dioxide capture and storage, there is an emerging need to reduce the emission of CO_2 to the atmosphere. In principle, three possible routes can be envisioned focusing on (1) the reduction of the energy consumption, (2) the efficient use of energy sources (if desired combined with capture and storage of CO_2), and (3) the use of alternative energy sources with reduced or no CO_2 emission. In addition to

*Corresponding author.
E-mail address: d.c.nijmeijer@utwente.nl

Sustainability Science and Engineering, Volume 2 ISSN 1871-2711, DOI 10.1016/S1871-2711(09)00205-0

that, the limited amount of fossil fuels forces the developments in the direction of alternative energy sources.

Salinity gradient energy has a huge potential as alternative and sustainable energy source. It uses the Gibbs energy of mixing of two salt solutions with different concentrations to generate electrical energy. It is a nonpolluting (no emissions of CO_2, SO_2, or NO_x), sustainable technology to generate energy by mixing water streams with different salinity. Salinity gradient power is available worldwide, everywhere where salt solutions of different salinity mix, for example, where fresh river water flows into the sea, or where industrial brine is discharged. The estimated global energy potential from estuaries alone is estimated to be 2.6 TW [2], which is approximately 20% of the worldwide energy demand [3] and more than the global electricity consumption (2.0 TW).

Pressure-retarded osmosis (PRO) and reverse electrodialysis (RED) are the most frequently studied processes to extract the potential energy available from the mixing of freshwater and saltwater, although some other membrane-based processes are proposed as well. In PRO, two solutions of different salinities are brought into contact by a semipermeable membrane that only allows the transport of the solvent (water) and retains the solute (dissolved salts). In RED, a number of anion and cation exchange membranes (CEM) are stacked together in an alternating pattern between an anode and a cathode and allow the selective transport of salt ions only.

Although the potential of salinity gradient power was already recognized in the 1950s [4], until now, commercialization and industrial use are still limited; however, several initiatives are currently employed for pilot plant construction and upscaling of both technologies (see later in this chapter).

This chapter describes the process of salinity gradient energy and its potential. It first gives a thermodynamic overview of the theoretical amount of energy available from the mixing of a diluted and a concentrated salt solution, which in principle is independent of the used technology (PRO or RED). After that, the chapter continues with a section especially dedicated to PRO and a section only focusing on RED. Both sections describe the principle and theory of the specific technology and are followed by a detailed description of the literature and membranes used for PRO or RED. It also mentions the challenges for membrane development in this respect. After that, both sections address process design considerations. The last part of both sections is dedicated to the upscaling and commercialization of both processes. The chapter finally ends with some concluding remarks.

2. THEORETICAL POTENTIAL OF SALINITY GRADIENT ENERGY

The driving force for transport of a component in salinity gradient power is a gradient in Gibbs energy or a potential difference between the two salt solutions. The Gibbs energy of a system reflects that part of the energy of the system that is available for work. The total amount of energy available from mixing 1 m^3 of a concentrated and 1 m^3 of a diluted salt solution can be determined from the chemical potential difference of the system after mixing, subtracted by the chemical potential of the system before mixing (Fig. 1):

$$\Delta G_{\text{mix}} = G_{\text{b}} - (G_{\text{c}} + G_{\text{d}}) \tag{1}$$

where ΔG_{mix} is the change in Gibbs energy (J/mol) and G_{b}, G_{c}, and G_{d} are the Gibbs energies of the brackish, the concentrated, and the diluted solution, respectively (J/mol). The Gibbs energy of an ideal solution is equal to

$$G = \sum \mu_i n_i \tag{2}$$

where G is the Gibbs energy of the system (J/mol), μ_i the chemical potential of component i in the solution (J/mol), and n_i the number of moles of component i in the solution.

The chemical potential of a component i (μ_i) in an ideal solution can be written as (e.g., [5])

$$\mu_i = \mu_i^0 + \bar{V}_i \Delta p + RT \ln x_i + |z_i| F \Delta\varphi \tag{3}$$

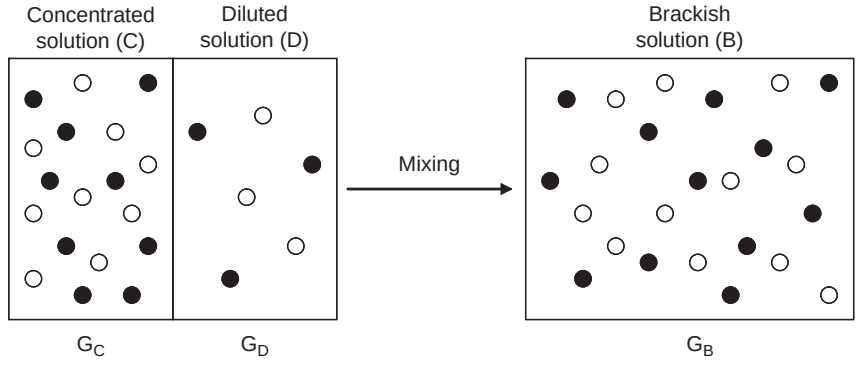

Figure 1 The mixing of a concentrated and a diluted solution to a brackish solution.

where μ_i^0 is the molar free energy under standard conditions (J/mol), Δp the pressure change compared to atmospheric conditions (Pa), $\bar{V}_i$ the molar or specific volume of component i (m^3/mol), R the universal gas constant [8.314 J/(mol K)], T the absolute temperature (K), x_i the mol fraction of component i, z the valence of an ion (eq/mol), F the Faraday constant (96,485 C/eq), and $\Delta\varphi$ the electrical potential difference (V). Since there is no pressure change or charge transport, when the concentrated and the diluted solution are mixed, Eq. (3) reduces to

$$\mu_i = \mu_i^0 + RT \ln x_i \tag{4}$$

When Eq. (4) is substituted in Eqs. (2) and (1), the standard chemical potential (μ_i^0) is eliminated and the final equation describes the Gibbs energy of mixing of a concentrated and a diluted salt solution:

$$\begin{aligned}\Delta G_{\text{mix}} &= \sum_i [G_{i,\text{b}} - (G_{i,\text{c}} + G_{i,\text{d}})] \\ &= \sum_i [\{(n_{i,\text{c}} + n_{i,\text{d}})RT \ln x_{i,\text{b}}\} \\ &\quad - (n_{i,\text{c}}RT \ln x_{i,\text{c}} + n_{i,\text{d}}RT \ln x_{i,\text{d}})]\end{aligned} \tag{5}$$

And when n is replaced by cV, this changes into

$$\begin{aligned}\Delta G_{\text{mix}} = \sum_i [&c_{i,\text{c}} V_{\text{c}} RT \ \ln(x_{i,\text{c}}) + c_{i,\text{d}} V_{\text{d}} RT \ \ln(x_{i,\text{d}}) \\ &- c_{i,\text{b}} V_{\text{b}} RT \ \ln(x_{i,\text{b}})]\end{aligned} \tag{6}$$

Because the mixing of two solutions is a spontaneous process, the Gibbs energy of mixing is negative: energy is released when two solutions are mixed. With Eq. (6), the theoretical available amount of energy available from the mixing of two salt solutions can be calculated and thus the theoretical potential of salinity gradient energy can be evaluated. This theoretically available amount of energy for an extensive range of sodium chloride concentrations is presented in Fig. 2 [3]. (*Note*: Because the figure shows the theoretical amount of energy *available* from the mixing of a diluted and a concentrated solution, the energy has a positive sign.)

Fig. 2 shows an extensive range of salt concentrations and the theoretically available amount of energy that can be obtained from the mixing of the two solutions. Values as high as $\sim$17 MJ can be obtained, depending on the concentration difference between the two solutions. Of course, this amount of energy strongly depends on the difference in

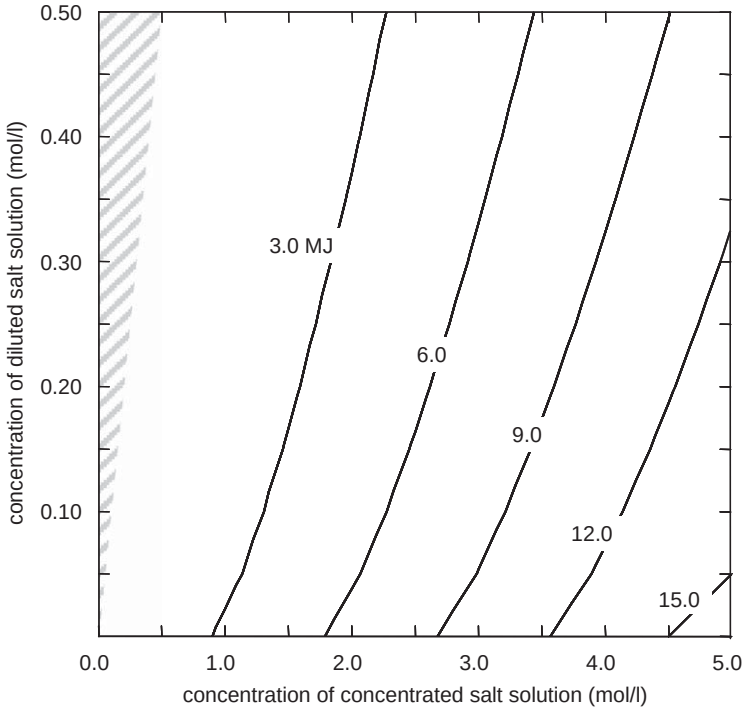

Figure 2 Theoretical available amount of energy (MJ) from mixing 1 m^3 of a diluted and 1 m^3 of a concentrated sodium chloride solution ($T = 293$ K). The shaded area is not taken into account because in this area the salt concentration of the concentrated solution is lower than that of the diluted solution [3].

concentration (or chemical potential) between the concentrated and the diluted salt solution. The higher this difference, the more energy can be extracted from the system. For example, the theoretically available amount of energy from mixing 1 m^3 seawater (comparable to 0.5 mol/L NaCl) and 1 m^3 river water (comparable to 0.01 mol/L NaCl) both at a temperature of 293 K is 1.7 MJ, whereas the theoretically available amount of energy from mixing 1 m^3 brine (5 mol/L NaCl) and 1 m^3 river water (0.01 mol/L NaCl) at 293 K is more than 16.9 MJ. When mixed with a large surplus of seawater, 2.5 MJ is theoretically available from 1 m^3 of river water (Table 1) [6]. Table 1 shows the amount of Gibbs energy theoretically available from the mixing of different volumes of a diluted and a concentrated salt solution [6]. This table clearly shows that when the amount of saltwater limits the process, the use of an excess of river water can be very beneficial

Table 1 Gibbs energy theoretically available from mixing different volumes of NaCl solutions at 298 K [6]

V_d (m^3)	V_c (m^3)	ΔG_{mix} (MJ)
∞	1	∞
10	1	6.1
2	1	2.8
1	1	1.76
1.26	0.74	1.87
1	2	2.06
1	10	2.43
1	?	2.55

V_d is the volume of the diluted solution (0.01 M NaCl), V_c the volume of the concentrated solution (0.5 M NaCl), and ΔG_{mix} the change in Gibbs energy.

(compare an available amount of energy of 6.1 MJ at $V_d = 10\,m^3$ and $V_c = 1\,m^3$ to an available amount of energy of only 1.76 MJ when both V_d and V_c are $1\,m^3$).

Although the above-presented equations provide a good first approximation for the theoretical amount of energy obtainable from salinity gradient energy, the calculations assume that the feed solutions consist of pure sodium chloride and behave ideal (no distinction between concentrations and activities). In practice, however, sea and river water are much more complex solutions and do not behave ideal, which makes the calculations much more complex. The numbers presented here represent the theoretical, maximum amount of energy available from the mixing of fresh and saltwater. Of course, in practice, it will not be possible to harvest this total theoretically available amount of energy, due to for example, mass transfer limitations, pressure drop, nonideal behavior, and so on. In addition, depending on the location and situation, there can be also several other limitations to use the total resources available, which are related to, for example, environmental impact, shipping, recreation, and tourism. But even if only part of the available energy can be recovered, the potential of salinity gradient energy remains huge.

3. PRESSURE-RETARDED OSMOSIS

3.1 Introduction

In PRO, the free energy of mixing from two solutions with different salinity is converted into energy by water transport through a semipermeable membrane from the diluted solution to the concentrated solution. In literature, PRO is defined as [7] ''The process of osmosis through a semipermeable membrane at a hydrostatic pressure difference between 0 and the osmotic pressure difference of the separated solutions, which generates a water flux against the hydrostatic pressure difference.'' This transport of water causes an increase of the pressure of the concentrated solution, which can be converted into electrical energy. Much of the pioneering work is published by Loeb [7–12] and Metha [9,13–15] and coworkers. They introduced the concept and published the first experimental results. Loeb et al. not only focused on the mixing of sea and river water, but also explored the possibility of applying PRO for the mixing of high saline solutions like Dead Sea water with seawater. Lee et al. [16] developed a theoretical model, which describes the PRO performance of a membrane based on osmosis and reverse osmosis (RO) measurements. They concluded that ''membranes with significantly improved performance will be needed if PRO is to become an economically feasible method for power generation using seawater–freshwater as the salinity gradient resource. However, the economics of a brine/freshwater system appear competitive with conventional power generation technologies.''

Due to ineffective membranes, which are the key component of PRO, not much effort took place to establish this technology. Since 1997, Statkraft, a Norwegian energy company, is engaged in the development of PRO [17]. They expect that the cost of osmotic power production will be in line with the cost of offshore wind generation and below wave and tidal power generation in 2010–2015. Statkraft is targeting for a membrane with high water flux and a low salt permeability. The performance of such a membrane should be close to 5 W of power generated per square meter of membrane area (W/m^2). Statkraft together with GKSS improved the performance of an asymmetric cellulose membrane from 0.6 to 1.3 W/m^2 [18]. Over 50 support materials have been tested for the development of a thin film composite membrane, which resulted in a power increase from 0.1 to 3.5 W/m^2 [18]. It is believed that the performance of these membranes could be improved even further. McCutcheon and Elimelech demonstrated the importance of a hydrophilic support for osmotically driven processes [19]. A hydrophobic support layer significantly hinders the

water flux not only through increased internal concentration polarization phenomena but also through disrupting the pathway by poor wetting of the structure. Recently, Thorsen and Holt [20] presented improved experimental results for PRO. They determined the PRO performance of a commercial cellulose acetate membrane without fabric reinforcement and obtained a power density of 1.6 W/m^2 for a solution containing 23.5 g/L NaCl. They predict for this membrane a power density of 2.1 W/m^2 for a 28.0 g/L NaCl solution. Even a much higher power density was obtained for a thin film composite membrane developed by GKSS [18], 2.7 W/m^2 for a 30.6 g/L NaCl [20]. This is a large increment in the performance of PRO.

Water transport from a less concentrated solution toward a more concentrated solution also occurs in forward osmosis (FO). There are many similarities in the desired membrane properties of FO and PRO and both aim for a highly selective membrane with a high water flux. In FO, an artificial salt solution (also called draw solution) is used to create a driving force for water transport through a semipermeable membrane. FO is used to recover the water from a saline or polluted water source. An advantage of this process is that no pressure is applied in FO equipment. The draw solution is either consumed (glucose/fructose draw solution), discarded, or regenerated and separated from the product water. Most of the recent work on FO is published by Elimelech and coworkers [21–26]. FO can also be used with the effluent of a freshwater sewage treatment plant and seawater (draw solution) [27]. In this case, the seawater is diluted with the water of the sewage treatment plant and is easier to treat due to its lower osmotic pressure.

3.2 Principle

In PRO, solutions of different salt concentrations are brought into contact through a membrane that allows the transport of water and retains the passage of salts. The chemical potential difference between both solutions creates a driving force [Eq. (5)]; water diffuses from the less concentrated solution through the membrane toward the concentrated salt solution, equalizing the chemical potential difference. If the concentrated solution is pressurized, then the transport of water would be lowered until the pressure reaches the osmotic pressure between both solutions. If the saltwater compartment would be further pressurized, RO would occur: transport of water from the concentrated salt solution toward the freshwater side. This process is schematically depicted in Fig. 3.

In PRO, the pressure on the concentrated salt solution is partly retarding the water flow through the membrane. This higher pressure allows the generation of electricity by a turbine.

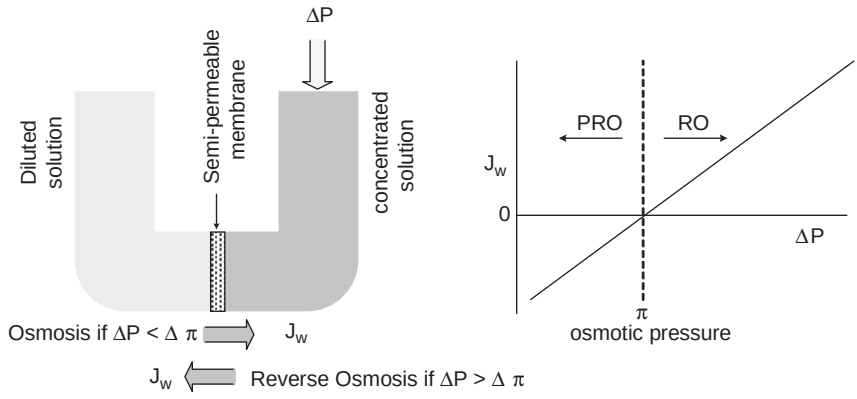

Figure 3 Transport of water (J_w) through a semipermeable membrane. If the hydrostatic pressure (P) on the concentrated solution is larger than the osmotic pressure (Π) transport of water from the concentrated solution to the diluted solution occurs (reverse osmosis). If the hydrostatic pressure is lower than the osmotic pressure, water is transported toward the concentrated solution. The increase in pressure at the concentrated solution can be converted into energy.

The osmotic pressure of a solution can be calculated by the van't Hoff equation:

$$\Pi = c_j R T \tag{7}$$

where c_j is the concentration of the solute (mol/m^3), R the universal gas constant [J/(mol K)], and T the absolute temperature (K). When the solute dissociates, the osmotic pressure increases proportionally. The osmotic pressure of a 35 g/L NaCl solution (comparable to seawater) is equal to 29.7 bar.

3.2.1 Concentration polarization

Fig. 4 shows the transport of water and salt through a semipermeable membrane in PRO. The membrane consists of a thin selective top layer supported by a porous support. The selective layer faces the high-pressure side in order to prevent release of the selective top layer from its support due to the pressure differences.

Because the membrane is not 100% selective, some salt will also be transported from the saltwater side to the freshwater side. In RO the transport of salt and water are in the same direction.

In PRO water is transported from the low-pressure freshwater side to the high-pressure saltwater side due to the osmotic pressure difference.

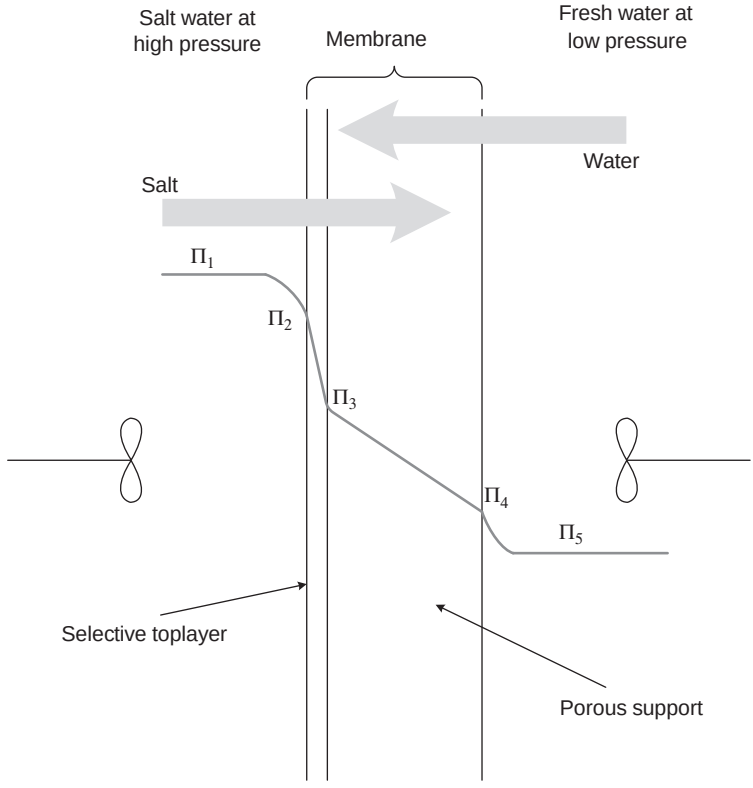

Figure 4 Schematic representations of the osmotic profiles of a PRO membrane. Π_1 is the osmotic pressure of the bulk of the concentrated salt solution, Π_2 the osmotic pressure at the dense top layer of the membrane, Π_3 the osmotic pressure inside the membrane between the dense top-layer and the porous support, Π_4 the osmotic pressure at the surface of the membrane in the diluted solution, Π_5 the osmotic pressure in the bulk of the diluted solution.

However, salt is transported in the opposite direction due to its concentration difference. The salt transport is limited by several resistances: external concentration polarization due to stagnant layers caused by reduced mixing on the membrane surface at the saltwater side and the freshwater side; internal concentration polarization due to resistance against salt transport in the thin selective top layer of the membrane and in the porous support layer.

Intensified mixing due to high cross-flow rates at the membrane surface can lower external concentration polarization. Internal concentration polarization arises from the resistance against mass transfer that salt experiences from the dense top layer and the stagnant boundary layer in the porous support. This porous support creates a stagnant zone through

which salt can only be transported by diffusion. These resistances against salt transport lower the effective osmotic pressure (Π_2–Π_3) over the selective top layer of the membrane. A good PRO membrane has a thin high selective top layer with a high resistance for salt transport and a very open (preferably thin) support layer. Loeb et al. showed that the support has a large contribution to the overall transport resistance and that the removal of the nonwoven/woven support from the membrane caused a higher osmotic water flux through the membrane [11]. A capillary membrane (with a thin porous layer) might be very beneficial for PRO applications [16].

When external concentration polarization is neglected, then the water transport can be described as follows:

$$J_w = A(\Delta\Pi_{eff} - \Delta P) = A(\Pi_2 - \Pi_3 - \Delta P) \tag{8}$$

where J_w is the water flux through the membrane [$m^3/(m^2\,day)$], A is a specific membrane transport parameter [$m^3/(m^2\,day\,bar)$], Π the osmotic pressure (bar), and ΔP the pressure difference between the fresh and saltwater solution (bar).

The osmotic pressure Π_3 is not known but can be calculated from the salt leakage through the membrane. This can be described as follows:

$$-J_s = B(C_2 - C_3) \tag{9}$$

where J_s is the salt flux through the membrane [$mol/(m^2\,day)$], B the salt permeability constant (m/day), and C the concentration (mol/m^3).

This salt flux is negative since its transport is in the opposite direction of the water flow. In the porous support, the diffusion of salt is counteracted by the flow of water. The salt flux through the support can be written as follows:

$$-J_s = D_s\varepsilon\frac{dC(x)}{dx} - J_w C(x) \tag{10}$$

where D_s is the diffusion coefficient of the salt in the membrane substrate (m^2/s), ε the porosity of the membrane substrate (–), and x the thickness of the porous support.

Lee et al. [16] solved this problem resulting in

$$J_w = A\left(\pi_2\frac{1-(C_4/C_2)\exp(J_w K)}{1+(B/J_w)(\exp(J_w K)-1)} - \Delta P\right) \tag{11}$$

For the special case of $C_4 = 0$ with only water on the freshwater side of the membrane reduces Eq. (11) to

$$J_w = A\left(\frac{\pi_2}{1 + (B/J_w)(\exp(J_w K) - 1)} - \Delta P\right) \tag{12}$$

Both equations can be solved numerically. In these equations A and B can be obtained from RO experiment, concentrations are known and J_w is measured during osmosis experiments allowing for the determination of K. K (s/m) refers to the solute diffusion in the porous support structure and is given as

$$K = \frac{t\tau}{D_s \varepsilon} \tag{13}$$

where t is the thickness of the membrane (m), τ the tortuosity of the pores in the support (–), D_s the solute diffusion coefficient (m^2/s), and ε the porosity of the membrane (–).

Eq. (11) can be further simplified by assuming that $\pi_2/\pi_4 = C_2/C_4$ [6] resulting in

$$K = \frac{1}{J_w}\left(\ln\frac{B + A\pi_2 - J_w}{B + A\pi_4}\right) \tag{14}$$

This equation is valid when the concentrated salt solution is facing the active dense layer. If the concentrated salt solution is facing the porous support, which is sometimes applied in FO [24], then the following equation is valid:

$$K = \frac{1}{J_w}\left(\ln\frac{B + A\pi_4}{B + J_w + A\pi_2}\right) \tag{15}$$

3.3 Membranes for pressure-retarded osmosis

PRO is the most studied membrane technology exploiting a salinity gradient. However, the amount of experimental data is scarce and difficult to compare with each other. Metha and Loeb and recently Thorsen and Holt [20] are the only authors who published experimental determined power densities for PRO at real conditions. Some PRO values are determined from osmosis experiments without applying a hydrostatic pressure. Such a pressure can have a significant effect on the water flux, since a very open support structure allows a high water flux, but is also susceptible to

compaction. Table 2 shows the available experimental results obtained from literature.

The reported power densities in Table 2 are derived from the reported flux and feed pressure. All the experimental results were obtained by Loeb and Metha from 1976 to 1982 and mainly for concentrated salt streams [8,9,14,15] and from Thorsen and Holt (2009) [20]. Loeb and Metha determined only one value (0.21 W/m^2) obtained for a feed concentration of 30 g/L NaCl, which represents seawater. Furthermore, it should be noted that the feed pressure is not chosen optimal [half of the osmotic pressure as indicated in Eq. (18)] necessary for a maximal power density. However, Thorsen and Holt [20] systematically varied the feed pressure and obtained for a NaCl concentration representing seawater the highest reported power densities 1.6 W/m^2 for a cellulose acetate membrane and 2.7 W/m^2 for a thin film composite membrane. Higher power densities (1.76–5 W/m^2) can be obtained for concentrated brine streams. However, the performance of the fibers deteriorates when exposed to high salt concentrations, probably caused by a change in the porous substructure. Based on Table 2 no clear conclusion can be drawn for the optimal membrane properties for PRO, mostly because the experimental conditions are difficult to compare with each other because of different process condition: feed pressure, salt concentration, and flow rates (external concentration polarization).

Proper PRO experiments are difficult to perform: feed pressure chosen should be optimal, feed flow rate should be high in order to minimize concentration polarization, and the amount of permeated water should be determined accurately. Therefore, Lee et al. [16] generated a theoretical model in order to predict the PRO performance from osmosis experiment [parameters A and B in Eqs. (8) and (9)] and from direct osmosis (K derived from the osmotic flow) as input parameters for their model. The results of direct osmosis experiments might be too optimistic, since these experiments do not take compaction phenomena into account [16]. The results of Lee et al. [16] and Loeb et al. [11] are shown in Table 3.

All the membrane parameters from Table 3 are derived from experiments with NaCl solutions, except for the Toray CA-3000 values, which were determined with $MgCl_2$. These latter values might be too optimistic since the parameters B and K depend on the type of salt. The asymmetric membranes show a higher performance compared to the composite membranes. These composite membranes have a lower projected power density due to their denser support layer, resulting in a high K value [16]. The retention and the resistance of the support layer play a crucial role in

Table 2 Measured PRO performance for various membranes at different feed concentrations and pressures for the mixing with freshwater (0 g/L NaCl)

Membrane	Type	Concentration feed		Water flux [$m^3/(m^2\,d)$]	P_{feed} (bar)	Power (W/m^2)	Reference
		NaCl (g/L)	Π_{feed} (bar)				
Du Pont permasep B-10	Asymmetric polyamide fiber	96	81	0.056	41	2.62	[14]
		108	91	0.042	51	2.46	
		143	122	0.070	51	4.10[a]	
		191	162	0.084	51	4.90[a]	
		191	162	0.081	51	4.77[a]	
		96	81	0.038	41	1.78[a]	
		96	81	0.070	41	3.26[b]	
		96	81	0.081	20	1.90[b]	
		143	122	0.045	61	3.17[b]	

FRL thin film composite	Composite polysulfone with furan skin fiber	72	61	0.032	3	0.11	[9]
		24	20	0.006	3	0.02	
		119	101	0.070	19	1.56	
UOP CA/SW	Asymmetric cellulose acetate flat sheet spiral wound	47	40	0.035	21	0.85	[15]
		94	80	0.090	21	2.14	
		139	118	0.081	24	2.26	
		51	44	0.037	21	0.89	
Du Pont permasep B-10	Asymmetric polyamide fiber	239	203	0.100	30	3.52	[8]
		119	101	0.050	30	1.76	
		30	25	0.012	15	0.21	
Osmonics SS10	Asymmetric cellulose acetate	23.5	16	0.390	8	1.60	[20]
Thin Film Composite	Composite	30.6	21.5	0.229	12	2.70	[20]

[a] Change in performance when $\Pi_f - P_f > 50$ bar.
[b] Different module.

Table 3 Calculated power densities (W/m^2) for various membranes derived from osmosis experiments (*A* and *B*) and osmosis experiments (K)

Membrane	Type	Membrane parameters						Projected	Reference
		A [m^3/(m^2 day bar)]	B (m/day)	K (day/m)	$\Delta P_o/\Delta\pi$	$\Delta P_o/2$ (bar)	J_w [m^3/(m^2 day)]	W_{max} (W/m^2)	
CA-80	Asymmetric	0.0088	0.173	0.75	0.88	12.60	0.109	1.59	[16]
CA-70	Asymmetric	0.0289	7.517	0.44	0.23	3.31	0.092	0.35	[16]
BM-05	Asymmetric	0.0035	0.020	21.99	0.70	9.90	0.028	0.32	[16]
PBIL	Asymmetric	0.0057	0.028	7.99	0.82	11.66	0.060	0.81	[16]
PA-300	Composite	0.0096	0.015	65.97	0.51	7.23	0.020	0.17	[16]
NS-101	Composite	0.0105	0.038	335.65	0.07	1.03	0.003	0.00	[16]
BM-1-C	Composite	0.0072	0.053	46.30	0.29	4.14	0.015	0.07	[16]
Toray CA-3000[a]	Asymmetric	0.0324	0.018	104.00	0.34	4.88	0.014	0.08[a]	[11]
Toray CA-3000[a]	Asymmetric without support fabric	0.0324	0.018	17.00	0.76	10.84	0.115	1.45[a]	[11]

[a] Values determined with $MgCl_2$ too optimistic for NaCl.

the performance of a PRO membrane. As can be seen from Table 3 membranes with a low water permeability (A) but with a high selectivity toward salts (low B) and an open support structure (low K) can exhibit a high power density (CA-80 membrane). A membrane with a high selective top layer for salts and an open porous support allow a higher optimal pressure stemming from a larger osmotic pressure difference over the selective layer of the membrane.

Support layers have a tremendous effect on the performance of a PRO membrane. The support layer should be as thin and open as possible without a support fabric. Asymmetric fibers are very attractive for PRO since they possess a thin porous support layer and no support fabric. However, these open structures should also be able to withstand the hydrostatic pressure during PRO operation and should not compact. Compaction of the open CA-80 fiber is observed by Lee et al. [16] and is not taken into account in their model. Real PRO experiments would most likely show a lower power density as compared to the values reported in Table 3.

Summarizing the optimal PRO membrane should have the following characteristics:

- A high water permeability [high A, Eq. (8)]
- Low salt permeability [low B, Eq. (9)]
- Low resistance in the porous support, very open or no support fabric [11] [low K, Eq. (13)]
- Hydrophilic porous support [19]
- Resistant against compaction
- Minimal external concentration polarization (high flow rates)

These parameters might be conflicting with each other and an optimal membrane is optimized with respect to these variables.

3.4 Process design

The basic process of an osmotic power plant is shown in Fig. 5.

A pressure exchanger is used in order to maintain a high pressure at the feed side of the membrane. The pressure of the brackish water leaving the system is used to pressurize the incoming seawater. The flows of the brackish water leaving the system and the seawater entering the system should be equal. The amount of water permeating through the membrane is used to generate electricity via a turbine. It should be noted that the pressure exchange should work very efficiently at low pressures (14.8 bar half the osmotic pressure) in order not to lose too much energy. Statkraft a Norwegian energy company found a very elegant solution for this problem by placing the osmotic power plant below sea level at such a depth that the

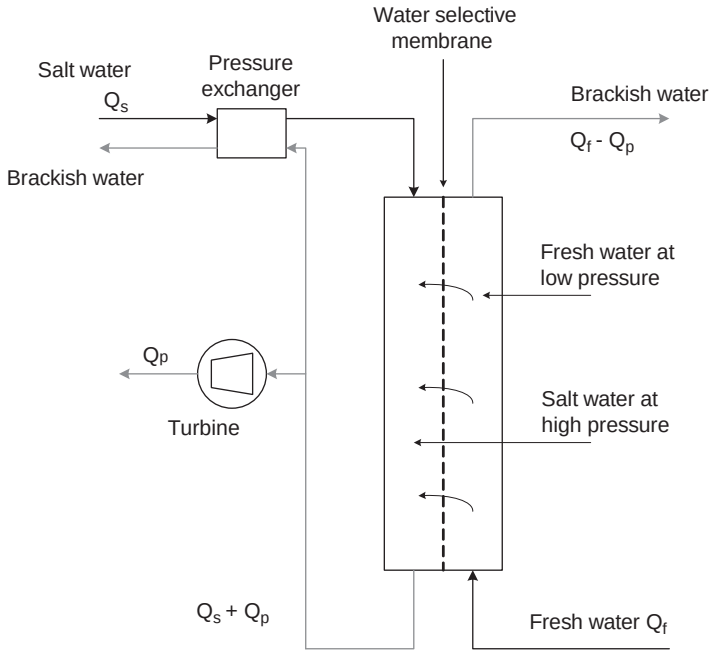

Figure 5 Basic principle of PRO water transport from freshwater toward a pressurized saltwater solution. *Q* is the flow of water (m^3/s), the subscripts f, s, and p stand for freshwater, seawater, and permeated water, respectively.

hydrostatic pressure equals the optimal operation pressure [Eq. (18)] for PRO [17,18].

The water selective membrane consists of a dense selective top layer (which is permeable for water and not for salts) and a porous support backing this thin layer. The selective top layer is facing the pressurized seawater.

The flux of water occurs due to an osmotic pressure difference between the freshwater and the saltwater and is retarded by the higher pressure of the saltwater. This can be described by the following relationship:

$$J_{H_2O} = A(\Delta\Pi - \Delta p) \tag{16}$$

where J_{H_2O} is the water flux in $m^3/(m^2\,s)$; A a specific membrane constant, $\Delta\Pi$ the osmotic pressure, and Δp the pressure difference between both solutions.

The amount of energy produced per square meter of membrane (E) is obtained by multiplying the water flux with the hydrostatic

pressure difference:

$$E = J_{H_2O}\Delta P \tag{17}$$

The maximal power density is obtained when $dE/dP = 0$, resulting in

$$\Delta P_{max} = \frac{1}{2}\Delta\Pi \tag{18}$$

which is the optimal pressure of the concentrated salt solution at the feed side of the membrane giving the highest power output. For PRO on river water and seawater this would mean an optimal pressure at the seawater side of 14.8 bar.

The maximal obtainable amount of power can be derived by substitution of ΔP_{max} in Eq. (17) resulting in

$$E_{max} = \frac{1}{4}A\Delta\Pi^2 \tag{19}$$

This equation clearly shows the effect of the osmotic pressure and membrane properties (A) on the energy production of PRO.

3.5 Pilot testing and upscaling[1]

Statkraft, an energy utility owned by the Norwegian government, is today the largest generator of renewable energy in Europe. With generation capacity within hydropower, wind power, gas power, and soon also solar power, the company has a large portfolio of environmental energy solutions. But it is clear to the company that to maintain a leading position within renewable energy it is necessary to focus on innovation with a clear ambition to deliver the energy solutions of the future. With over 100 years of tradition in hydropower, working with pressurized water and sustainable project development, it was natural that Statkraft turned the focus toward PRO already in 1997.

When Statkraft started working on PRO, the first efforts were to understand the realistic potential of this concept provided the technology would be made available. Calculations and surveys of the availability of the resources – freshwater and seawater – were executed, and the result showed that a significant amount of clean, renewable energy could be produced by

[1]The information given in this section is provided by and property of the company Statkraft AS, Norway and used with permission. The authors would like to acknowledge Statkraft AS for the contribution.

osmotic power. In addition, there are specific characteristics of this technology that give it its unique character not only among the new sources of renewable energy that are currently under development, such as tidal and wave power, but also in regard to more established technologies such as solar and wind. Since the generation of power is based on the availability of freshwater and seawater, resources that usually will be available all year round, osmotic power has the characteristics of a base load source of renewable energy. This is very different from the other technologies that are dependent on the present weather conditions, hence require back up supplies from other sources.

Another interesting characteristic is that after making a survey of the rivers running into the ocean worldwide, one found that these sites usually also have either settlements or industry, and mostly both. This means that the consumer of the electricity produced by osmotic power will be just next door to the power plant. When reflecting on the situation that most new sources of renewable energy, such as wind, wave, and so on, usually have huge challenges and significant investments related to the connection of the power generation device to the grid, this adds another advantage for the generation of osmotic power as a contribution to the total energy mix.

Based on the previously stated advantages of this new technology, Statkraft made a detailed study of the state of the technology necessary to exploit these possibilities of PRO. Although there is a lot of resemblance with components used in other processes, it became clear that the membranes are one of the crucial components, where significant improvements both in efficiency and in cost were necessary. The membranes produced at that time were not in a position to produce power at a competitive level. Hence extensive efforts to design a membrane suitable for PRO were made, and this was done together with partners with long experience in membrane development both in the United States and in Europe. As described earlier, this is not an easy task, but today the best results produced by Statkraft are in the range of 3 W/m^2. This result shows the significant progress made in membrane development and it made Statkraft to decide to expand their efforts to the maximum towards a full-scale osmotic power system.

In the fall of 2007, Statkraft decided, due to the promising improvement in the critical components, such as membrane and pressure recovery devices, the time had come for a full-scale proof of the concept for a complete PRO system. A plant with a sufficiently large amount of membrane area is currently built to transfer the salinity gradient into work and also further into electricity. At the same time, the interface for, and integration of, all the

components in the system can be studied together in operation, not only as individual parts of a system.

After a little more than a year of development and construction, the world's first prototype plant has been put into operation in spring 2009 in the southeast of Norway (Fig. 6). The location is within the facility of a pulp factory in operation, which simplifies the approval process and at the same time gives good access to the existing infrastructure. In addition, the location has good access to seawater from the ocean and freshwater from a nearby lake.

The prototype plant is designed as a typical plant placed at sea level. Freshwater is taken from a river close to its outlet. Seawater is fed into the plant by underground pipes, and the brackish water is led to the natural brackish water zone.

The main objectives of the prototype PRO plant are twofold. First, it confirms that the designed system can produce power on a reliable 24-h/day production. Second, the plant will be used for further testing of the technology achieved from parallel research activities to substantially increase the efficiency. These activities will mainly be focused on membrane modules, pressure exchanger equipment, and power generation (turbine and generator). In addition, there will be a focus on further development of

Figure 6 Prototype PRO plant at the east coast of Norway.

control systems, water pretreatment equipment, as well as infrastructure with regard to water inlets and outlets.

The plant is equipped with 2000 m^2 of specially designed PRO membranes. A miniature hydropower turbine and devices for recovery of hydraulic pressure are installed. Although the design capacity is in the range of 10 kW, the expectations for the capacity in the first phase are somewhat less. The membranes have room for improvement, and there are high expectations for optimizations for the full system as such.

Since this is the first plant built for PRO operation, several precautions have been taken to make sure that possible pollution in the water does not destroy the membranes (Fig. 7). For the seawater regular pressure screens are used, and for the freshwater from the lake the pretreatment is similar to that being used for drinking water. The ambition is that the freshwater can be treated similar to the seawater. This will however be based on the operational experiences.

After the start-up, operation, and further testing the experience gained will be based on both operational changes as well as changes to the system and replacement of parts. This is in order to increase the efficiency and optimize the power generation. In a longer perspective, this would be used as a basis to develop a power plant with an installed capacity between 1 and 2 MW, bringing the technology one step further toward commercialization.

The prototype plant put into operation during 2009 is also intended as a meeting place for parties from both government and industry with ambitions in osmotic power. With the increasing focus on the environmental

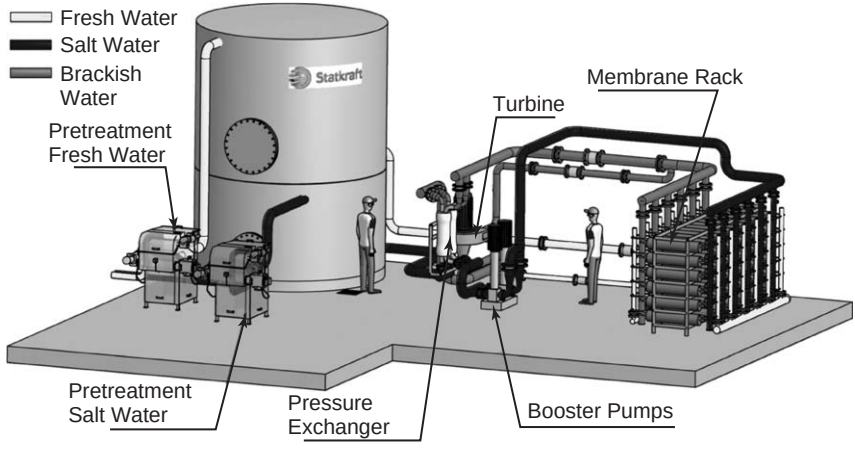

Figure 7 Prototype PRO plant illustration.

challenges and the need for more renewable energy, this can give a significant contribution to increase the momentum in development of new clean technologies.

Statkraft has specified that in order to be competitive to other new, renewable sources of energy, a power output of 5 W/m^2 for flat-sheet membranes is required, whereas due to the higher packing densities obtainable, a target in the range of 3 W/m^2 should be sufficient for hollow fiber membranes. This is based on the water flux trough the membrane, in relation to the salt retention that creates the driving force. The estimated costs of producing one MW based on a number of detailed investment analyses are that osmotic power will be able to produce electricity at a cost level of Euro 50–100 MW^{-1}, which is in a similar range as other renewable technologies such as wind power, wave and tidal power, and power based on biomass.

These calculations are based on existing hydropower knowledge, general RO desalination engineering information, and with a membrane target as a prerequisite. The capital costs of installed capacity are high compared to other renewable energy sources. However, each MW installed is very productive, with an average operation time above 8000 h a year. This should generate approximately twice the energy supplied (GWh) per installed MW per year compared to a wind mill.

To achieve competitiveness, given the large volumes of membranes, the membrane pricing is important. For an average 25 MW plant, it is calculated that 5 million m^2 of membrane area is required, meaning that the industry would see a demand of PRO membranes exceeding the current RO membrane market.

There are still significant improvements and verifications of the technology required before osmotic power can be represented among the currently commercial renewable energy technologies. But it is not only the technology itself that need to be put into place to exploit this huge potential; in the following sections some of the major topics to be assessed will be discussed, and it is known from the history of developing both wind power and solar power that these topics are not trivial. For wind and solar power, the technology was long past the proof of concept, but it took still several decades before these were able to gain a significant market share.

A new technology such as osmotic power can only be developed to a certain level by researchers and especially dedicated companies such as Statkraft. But to exploit the full potential of such a technology, one will be dependent on external factors as well, such as that several organizations have sufficient demand for this specific power technology. When several

companies and governments around the world commit themselves to utilize the technology, whether it is solar, wind, or osmotic power, this provides strong signals to the supplier industry and the competition for developing and supplying the best solution will go up to full speed.

4. REVERSE ELECTRODIALYSIS

4.1 Introduction

In RED, the energy of mixing two solutions with different salinity is extracted through the transport of ions (this in contrast to PRO, where the transport of water accounts for the generation of power). Pattle was the first researcher who proved the principle of RED [4]. With his pioneering work, he was the first one to be able to generate power from the mixing of fresh and saltwater through the selective transport of ions. In the 1970s, Weinstein and Leitz [28] investigated the effect of the composition of the salt solutions on the power output. The main conclusion of their work was that large-scale application of RED could become feasible, but only if major improvements regarding the manufacturing of ion exchange membranes and careful optimization of the operating conditions are possible. In the early 1980s, Lacey [29] prepared a comprehensive review on RED and concluded that to make RED economically viable minimization of the internal stack resistance and maximization of the net power output from the cell are a prerequisite for success. The main conclusion of Lacey's work is that membranes for RED should have a low electrical resistance and a high selectivity combined with a long service life time, acceptable strength, dimensional stability, and low costs. In the early 1980s, Audinos [30] compared two different types of electrodialysis membranes for their applicability in RED (one pair of homogeneous and one pair of heterogeneous membranes) and investigated the effect of the type of salt solution (NaCl vs. $ZnSO_4$). The maximum power output obtained was 400 MW/m^2. In the mid 1980s, Jagur-Grodzinski [31] investigated the effect of hydrodynamics, that is, different salt solution streams and membrane spacer modifications, as a method to increase the power output. Although promising, the number of papers on RED in the 1990s and in the beginning of the 21st century was very limited. However, since a few years RED has been recognized again as a potentially attractive technology for the production of sustainable energy and as such it has regained the interest of many researchers [32–39], industrial partners, and the public. In this part, we first discuss the principle and the fundamentals of RED. It continues with a closer look at the membranes used for RED.

After that we focus on the different elements in RED, which are subsequently the membranes and the feed compartments including spacers. Although electrodes and electrode reactions are also major elements in a RED stack, the available literature and research on this topic is very limited, and therefore this topic will not be addressed here. This part is followed by a paragraph that focuses on process and stack design. This chapter finally ends with a description of the state-of-the-art and current status of RED and also gives a glimpse on pilot testing and upscaling.

4.2 Principle

In RED, a concentrated salt solution and a less concentrated salt solution are brought into contact through an alternating series of anion exchange membranes (AEM) and CEM (Fig. 8).

The concentrated and the diluted salt solution are separated by an alternating series of AEMs and CEMs. The AEM contain fixed positive charges and only allow the selective transport of anions toward the anode, whereas the CEM contain fixed negative charges and only allow the selective passage of cations towards the cathode. Both the concentrated

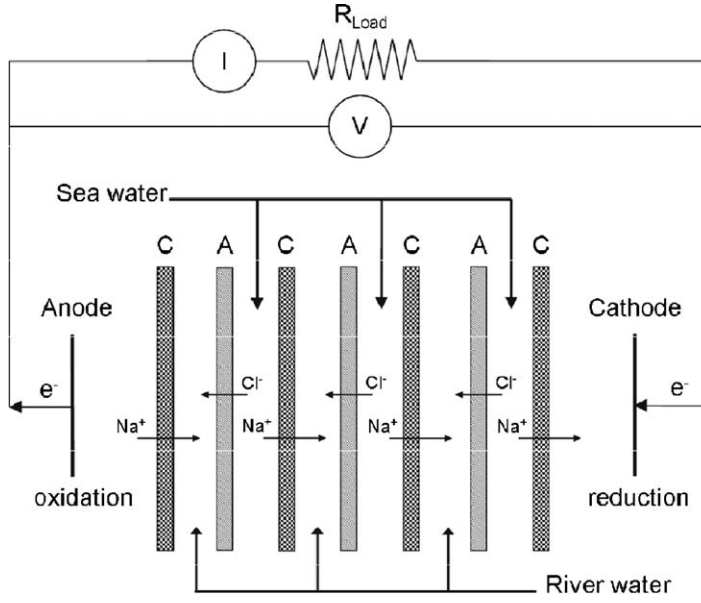

Figure 8 Principle of RED. *A* is an anion exchange membrane, *C* a cation exchange membrane, *V* the potential difference over the applied external load (V), *I* the electrical current (A) and R_{Load} the resistance of the external load (Ω). A redox couple is used at the electrodes to mitigate the transfer of electrons from anode to cathode [34].

and the diluted feed compartment contain a spacer to control the hydrodynamics. The electrons released at the anode are subsequently transported through an external circuit containing an external load, to the cathode. In the internal circuit in the stack, charge is carried by ions, while in the external circuit, electrons carry the charge. The ionic current is converted into electrical current by redox reactions that occur at the electrodes at the outer side of the stack. The redox couple is used to mitigate the transfer of electrons. A typical redox couple currently often used for RED is a solution of $K_4Fe(CN)_6$ and $K_3Fe(CN)_6$ (potassium iron(II) hexacyanoferrate and potassium iron(III) hexacyanoferrate) in a bulk solution of NaCl. At the cathode, the iron(III) complex is reduced and the iron(II) complex is reoxidized at the anode:

$$Fe(CN)_6^{3-} + e^- \leftrightarrow Fe(CN)_6^{4-} \quad E_0 = 0.36\ \text{V}$$

The solution is recirculated between both electrode compartments to maintain the original iron(III)/iron(II) ratio.

The chemical potential difference between the two salt solutions with different concentrations is the driving force for this process and generates a voltage difference over each pair of membranes. The theoretical value of this potential difference over the membrane for an aqueous monovalent electrolyte (e.g., NaCl) can be calculated using the Nerst equation:

$$\Delta V_{\text{theo}} = \frac{RT}{zF} \ln\left(\frac{a_c}{a_d}\right) \tag{20}$$

where ΔV_{theo} is the theoretical membrane potential for a 100% selective membrane (V), R the universal gas constant [8.314 J/(mol K)], T the absolute temperature (K), z the electrochemical valence, F the Faraday constant (96,485 C/mol), a_c the activity of the concentrated salt solution (mol/L), and a_d the activity of the diluted salt solution (mol/L). For freshwater (0.017 M NaCl, $\gamma_{\pm} = 0.878$) and seawater (0.5 M NaCl, $\gamma_{\pm} = 0.686$), the theoretical voltage difference per membrane is 80.3 mV. The overall, total potential of the system is the sum of the potential differences over each pair of membranes (e.g., 100 membrane pairs provide a voltage difference of $100 \times 80.3 = 8030$ mV or 8 V).

The power density obtainable from RED (defined as the power generated per unit of total membrane area) is equal to the product of half the current and the potential difference over an external load (comparable to PRO, where the power is equal to the product of the

pressure and the flux):

$$P^{\mathrm{RED}} = \frac{I}{2}\Delta V = \frac{1}{2r}(\Delta\phi - \Delta V)\Delta V \tag{21}$$

where P^{RED} is the power density obtainable in RED ($\mathrm{W/m^2}$), ΔV the potential difference over an external load (V), r the area resistance ($\Omega\,\mathrm{m^2}$), and $\Delta\phi$ the electrochemical potential difference between the two solutions (V). The maximum power density obtainable from RED can be calculated when Eq. (21) is differentiated with respect to the potential difference over the external load. At the maximum power output, $\mathrm{d}P/\mathrm{d}\Delta V$ is 0 and, as a result, the maximum power output can be obtained when ΔV is equal to $\Delta\phi/2$. In this situation, when substituting this value of ΔV in Eq. (21), the maximum power density obtainable is equal to

$$P^{\mathrm{RED}} = \frac{1}{2r}\frac{\Delta\phi^2}{4} \tag{22}$$

4.3 Membranes for RED

In 2007, Turek [32] studied the effect of the solution velocity on cell power output and process economy and observed that the main bottleneck for successful market introduction of RED is the membrane price. Nevertheless, most of the earlier work was dedicated to stack design and the effect of solution flow and composition, but not to ion exchange membrane characterization and performance testing. Ion exchange membranes are membranes with fixed anionic or cationic exchange groups that are able to transport cations or anions. The presence of these charged groups gives these membranes their specific properties and amount, type, and distribution of the ion exchange groups determine the overall membrane properties. Based on the type of fixed charge groups, ion exchange membranes can be classified as strong acidic and strong basic, or weak acidic and weak basic membranes. In strong acidic CEMs, sulfon groups serve as the fixed charged group in the membrane. Weak acidic membranes contain carboxylic acid as the fixed charged group. Quaternary and tertiary amines, respectively, provide the fixed positive charged groups in strong and weak basic AEMs (Fig. 9).

Two different types of ion exchange membranes can be distinguished, a classification that is based on the structure of the membrane: homogeneous and heterogeneous membranes. In homogenous ion exchange membranes, the fixed charge groups are evenly distributed over the entire membrane matrix. Homogenous membranes can be manufactured by polymerization

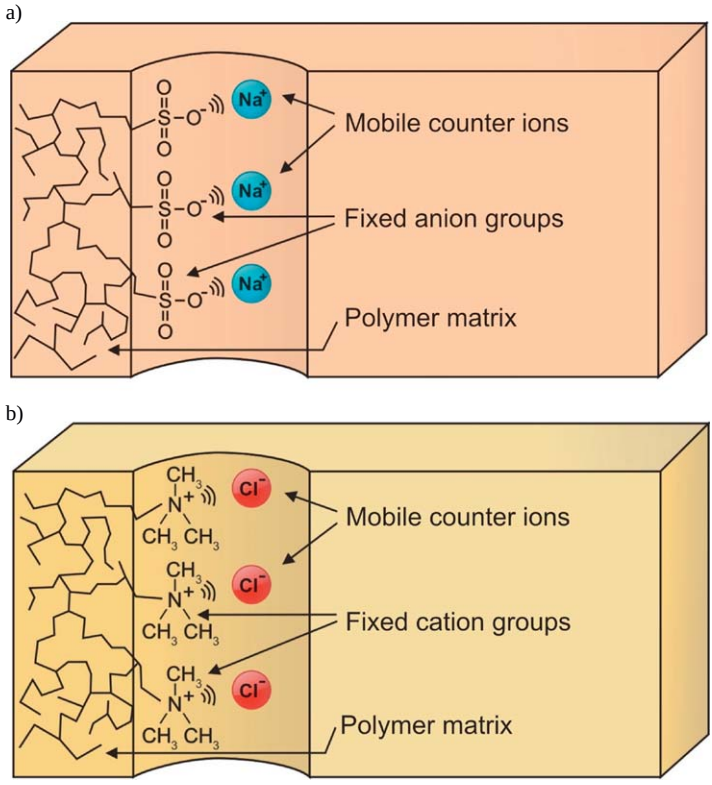

Figure 9 Typical example of (a) a cation exchange membrane (CEM) with SO_3^- groups as the cation exchange group and (b) an anion exchange membrane (AEM) with $N(CH_3)_3^+$ as the typical anion exchange group.

and polycondensation of functional monomers (e.g., fenylosulfonic acid with formaldehyde) or functionalization by, for example, postsulfonation [40–43]. Heterogeneous membranes have distinct macroscopic charged domains of ion exchange resins in a basically uncharged polymer membrane matrix. These membranes are usually produced by melting and pressing a dry ion exchange resin with a granulated polymer (e.g., polyvinylchloride) [44] or by dispersing the ion exchange resin in a polymer solution [45]. The distinct difference in structure between homogenous and heterogeneous ion exchange membranes also influences the properties of the specific membrane, as will be shown later.

Ion exchange membranes are the key elements in RED and the electrical resistance of the membrane and its permselectivity (the ability of the membrane to discriminate between cations and anions) are the most

important membrane properties for RED because these properties directly influence the overall RED performance and power output. Because these properties are directly determined by the number of fixed charges inside the ion exchange membrane, the ion exchange capacity (IEC), the swelling degree (SD), and the fixed charge density of a membrane also play a crucial role.

The IEC [expressed in milliequivalent of fixed groups per gram of dry membrane (meq/g membrane)] is the number of fixed charges inside the ion exchange membrane per unit weight of dry polymer. The fixed charge density, expressed in milliequivalent of fixed groups per volume of water in the membrane (meq/L), is determined by this IEC and the SD of the membrane. The fixed charge density is lower in the swollen state than in the dry state because the distance between the charged groups is increased upon swelling of the membrane, while the number of charged groups remains unchanged. The concentration and the type of these fixed charged groups determine the electrical resistance and the permselectivity of the membrane, and these properties are directly related to the maximum power output obtainable in RED.

When an ion exchange membrane is in contact with an electrolyte (salt solution), ions with the same charge as the fixed charges in the membrane (co-ions) are excluded and cannot pass through the membrane, while the oppositely charged ions (counterions) can freely move through the membrane. This effect is known as Donnan exclusion [46]. Ion exchange membranes are never 100% selective and the permselectivity of an ion exchange membrane quantifies the ability of that membrane to discriminate between co-ions and the oppositely charged counterions.

Although the charge density has a strong influence on both the permselectivity and the membrane resistance, a straightforward relationship between the permselectivity and the membrane resistance does not exist as can be seen in Fig. 10 [32] (values for both AEMs and CEMs and homogeneous and heterogeneous membranes are shown).

In general, the resistance of heterogeneous ion exchange membranes is significantly higher than that of the homogenous types. This phenomenon can be related to the structure of the heterogeneous membranes: heterogeneous ion exchange membranes have distinct macroscopic domains of ion exchange resins in an uncharged polymer matrix. Consequently, the resistance of these heterogeneous membranes is higher. In general, less selective membranes have a lower membrane resistance than more selective ones, although this is only a general trend and several exceptions exist. In general, the permselectivity of CEMs is higher than the corresponding

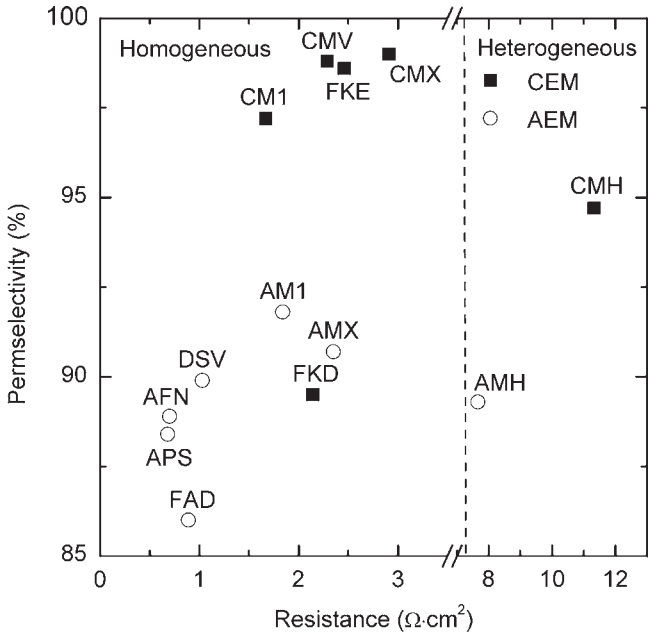

Figure 10 Membrane permselectivity as a function of the membrane resistance (at 25 °C). CEM is a cation exchange membrane (■) and AEM is an anion exchange membrane (□) [34].

values for AEMs. This is mainly due to the higher SD of AEMs, which reduces the effective fixed charge density and thus reduces the permselectivity.

Audinos [30], who was one of the first who systematically investigated the effect of two types of anion and CEM pairs on the power output in RED, already mentioned explicitly the importance of membranes specially developed for RED. Nevertheless, mainly due to limitations in availability of such membranes, most scientists use the above-presented standard electrodialysis membranes to study the performance of a RED system [30,31,38,47]. The manufacturer data available for these membranes do not offer sufficient information on the membrane properties relevant for RED and do not always allow mutual comparison of the different commercially available membranes, because of the different conditions often used for membrane characterization. Długołęçki et al. [34] made a comprehensive overview of membrane benchmarking for RED. They experimentally determined a range of membrane properties of commercially available membranes relevant for RED under equivalent conditions to enable a fair

comparison of the results and a proper evaluation of the different membranes for application in RED. Table 4 shows the experimentally determined values of these properties [34]. For comparison, the data of the manufacturers are also presented, although they are not always determined under equal conditions [48–51].

Table 4 clearly shows that the membrane characteristics vary over a wide range and strongly depend on the type of membrane and the differences in molecular structure and composition of the membranes. In general, the data provided by the manufacturers are in reasonable good agreement with the experimentally determined values, with some exceptions.

The IEC presented in Table 4 represent the number of strong acidic ($-SO_3^-$) groups in CEMs and strong basic ($-NR_3^+$) groups in the AEMs. Although the experimentally determined IEC is generally in good agreement with the data supplied by the manufacturers, strong deviations are visible for the APS membranes of Selemion and the FAD membranes from Fumasep. Both AEMs consist of a mixture of weak and strong ion exchange groups, but the experimental method used to determine the IEC only allows the detection of strong basic groups, whereas weak basic groups are not recognized. This results in significantly lower experimental values for the IEC, compared to the manufacturer's data. In general, SD values are similar to the data of the manufacturers, although the experimentally determined SD of the Selemion APS membrane is extremely high, which is probably due to the rough membrane surface of the APS membrane, which affects the wiping off of water from the membrane surface before measuring the weight. The thickness of the membrane strongly depends on the type of the membrane: Homogenous membranes are generally thinner than heterogeneous membranes, which is due to the structure of the membrane and its preparation method [40–43,52,53].

Based on these experimentally determined data, Długołęçki et al. [34] applied a theoretical model to evaluate these specific membrane properties in relation to the expected performance of these membranes under RED conditions [28,34]. This model relates the membrane resistance (R_{aem} and R_{cem}) and its permselectivity (α_{av}) directly to the maximum power output in RED [W_{max} (W)]. Membrane resistance and membrane permselectivity are the two most important parameters in this respect because they indirectly also include the membrane thickness and structure, its IEC and SD, and thus the fixed charge density:

$$W_{max} = NA \frac{\left[\alpha_{av} RT/F \ \ln(a_c/a_d)\right]^2}{R_{aem} + R_{cem} + (d_c/\kappa_c) + (d_d/\kappa_d)} \tag{23}$$

Table 4 Experimentally determined membrane characteristics of several commercially available ion exchange membranes (bold) [34]

Membrane	IEC (meq/g dry)		Permselectivity[a] (%)		Resistance[b] ($\Omega.cm^2$)		SD (%)		Thickness (μm)		Properties
Cation exchange membranes											
Fumasep®											
FKE	**1.36**	>1.0	**98.6**	>98	**2.46**	<3.0	**12**	15	**34**	50–70	Electrolysis, high selectivity
FKD	**1.14**	>1.0	**89.5**	>95	**2.14**	<3.0	**29**	25–30	**113**	90–100	Diffusion dialysis for NaOH
Neosepta®											
CM-1	**2.30**	2.0–2.5	**97.2**	>96[c]	**1.67**	1.2–2.0	**20**	35–40	**133**	120–170	Low electric resistance
CMX	**1.62**	1.5–1.8	**99.0**	>96[c]	**2.91**	1.8–3.8	**18**	25–30	**164**	140–200	High mechanical strength
Ralex® (Heterogeneous)											
CMH-PES	**2.34**	2.2	**94.7**	>92	**11.33**	<10	**31**	<55	**764**	<700	Electrodialysis, Electrodeionization
Selemion®											
CMV	**2.01**	N/A	**98.8**	>92	**2.29**	3.0[d]	**20**	N/A	**101**	130.0	Electrodialysis

Anion exchange membranes											
Fumasep®											
FAD	**0.13**	>1.5	**86.0**	>91	**0.89**	<0.8	**34**	25	**74**	80–100	Diffusion dialysis for acid
Neosepta®											
AM-1	**1.77**	1.8–2.2	**91.8**	>96[c]	**1.84**	1.3–2.0	**19**	25–35	**126**	130–160	Low electric resistance
AFN	**3.02**	2.0–3.5	**88.9**	>96[c]	**0.70**	0.4–1.5	**43**	40–55	**163**	150–200	Resistant against organic fouling
AMX	**1.25**	1.4–1.7	**90.7**	>96[c]	**2.35**	2.5–3.5	**16**	25–30	**134**	160–180	High mechanical strength
Ralex® (Heterogeneous)											
AMH-PES	**1.97**	1.8	**89.3**	>90	**7.66**	<8	**56**	<65	**714**	<850	Electrodialysis, Electro deionization
Selemion®											
DSV	**1.89**	N/A	**89.9**	N/A	**1.03**	1.0[d]	**28**	N/A	**121**	100.0	Diffusion dialysis, low resistance
APS	**0.29**	N/A	**88.4**	N/A	**0.68**	0.5[d]	**147**	N/A	**138**	150.0	Diffusion dialysis, oxidant proof

Note: For comparison the data given by the membrane manufacturers are also presented [48–51].
[a] Membrane potential measured across the membrane between 0.5 and 0.1 M solutions.
[b] Measured in 0.5 M NaCl solution at 25°C.
[c] Measured by electrophoresis, 2 mA/cm^2.
[d] Determined by 1 kHz AC measurement in the 0.5 N NaCl solution at 25°C.

where N is the number of membrane pairs (one cell pair consist of one anion and one CEM), α_{av} the average membrane pair permselectivity (–), R the universal gas constant [8.314 J/(mol K)], T the absolute temperature (K), F the Faraday constant (96,485 C/mol), a_c the concentrated solution activity (mol/L), a_d the diluted solution activity (mol/L), R_{aem} the AEM resistance ($\Omega\,m^2$), R_{cem} the CEM resistance ($\Omega\,m^2$), A the effective membrane area (m^2), d_c the thickness of the concentrated compartment (m), d_d the thickness of the diluted compartment (m), κ_c the concentrated compartment conductivity (S/m), and κ_d the diluted compartment conductivity (S/m).

In order to compare commercially available membranes with each other, it is more convenient to convert the power output into power density, which is the power output normalized for the membrane area (W/m^2):

$$P_{max} = \frac{W_{max}}{AN_m} \tag{24}$$

where P_{max} is the maximum power density (W/m^2), W_{max} maximum power output (W), A the effective membrane area (m^2), and N_m the number of membranes (–).

As Eqs. (23) and (24) predict the theoretical power output of the total system under RED conditions in relation to the individual membrane characteristics, it can be used as a tool to evaluate and compare the different anion and cation exchange membranes with respect to their performance in RED. Długołęçki et al. [34] evaluated the relative importance of membrane resistance and permselectivity on the power density in a RED stack. Fig. 11 shows the power density as a function of the membrane resistance and permselectivity for two different spacer thicknesses (a) 600 and (b) 150 μm.

When thicker spacers (> 600 μm, Fig. 11a) are used in the system, the power density of the system is hardly dependent on the membrane resistance or permselectivity. In this case, the resistance of the dilute compartment dominates the overall process resistance and maximum power densities of only 2 W/m^2 can be obtained. When the distance between the membranes is decreased (Fig. 11b), the effect of the membrane properties and thus the difference in power density of the different membranes becomes more pronounced. With increasing permselectivity and especially decreasing membrane resistance, the power density significantly increases and values as high as 7 W/m^2 can be obtained with properly designed stacks. Nevertheless, the process requires a minimum in spacer thickness

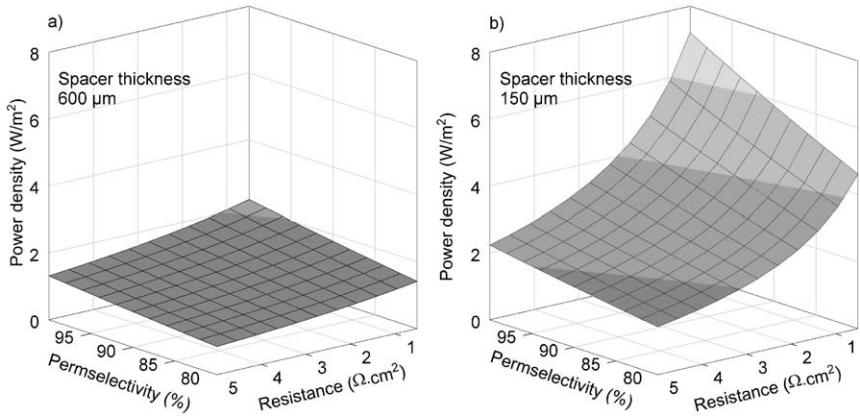

Figure 11 Relationship between the power density, the membrane permselectivity, and the membrane cell pair resistance for membrane pair with (a) 600 µm and (b) 150 µm thick spacers. Model calculations are based on seawater (0.5 M NaCl) as concentrated salt solution and river water (0.05 M NaCl) as diluted stream ($T = 25\,^{\circ}C$) [34].

because at too thin spacer thicknesses, the energy consumption for solution pumping increases tremendously due to the high pressure drop over the compartments.

Because Eqs. (23) and (24) can also be used to predict the performance of only a cation or only an AEM in RED, Długołęçki et al. [34] used their experimental data presented in Table 4 as input values for the model calculations to predict the maximum power density obtainable with each specific membrane (Fig. 12a and b). In this case, the average membrane pair selectivity (α_{av}) is replaced by the individual membrane selectivity of the cation or anion exchange membrane, respectively, whereas in the case of a CEM the corresponding resistance of the AEM is neglected, and vice versa when only an AEM is used. The thickness of the concentrated and diluted compartment is divided by a factor 2. Długołęçki et al. assumed that seawater has a NaCl concentration of 0.5 M ($\gamma_{\pm} = 0.686$ and $\kappa_c = 4.648$ S/m, $T = 25\,^{\circ}C$) and river water has a concentration of 0.05 M NaCl ($\gamma_{\pm} = 0.820$ and $\kappa_c = 0.551$ S/m, $T = 25\,^{\circ}C$).

It is obvious that the power density strongly depends on the spacer thickness (as presented before) and also on the type of membrane. The resistance of the heterogeneous membranes investigated is too high to be useful in RED. Even in a perfectly designed RED stack (extremely thin spacers), it is not possible to obtain power densities higher than 1.5 W/m^2.

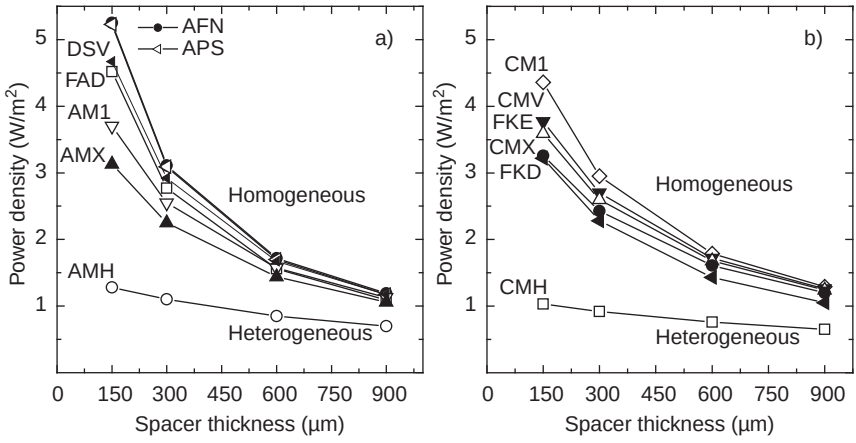

Figure 12 Prediction of the maximum obtainable power density based on experimental membrane characterization for (a) anion exchange membranes and (b) cation exchange membranes [34].

Homogeneous membranes are more suitable for RED. Based on these results, the best benchmarked AEMs are Neosepta AFN from Tokuyama Co. (Japan) and Selemion APS from Asahi Glass Co. Ltd. (Japan), with a predicted power density of more than 5 W/m^2 (at a spacer thickness of 150 μm). The Neosepta CM-1 CEM from Tokuyama Co. (Japan) shows the best performance as CEM for RED and reaches a theoretical power density of more than 4 W/m^2.

Although this model is a very useful tool to make a rough estimation of the performance of the different membranes under RED conditions, it is a theoretical model that includes several assumptions [34]: (i) concentration polarization phenomena near the membrane surface are negligible due to the small current densities obtained through the membranes and (ii) the resistance of the electrodes is assumed to be negligible compared to the membrane resistance. This assumption is allowed when the resistance of the membranes is large compared to the resistance of the electrodes, which can be obtained when a large number of membrane cell-pairs is used (as will be required anyway to generate sufficient power at low costs), and (iii) the feed solution does not change in concentration along the channels. This assumption has a strong relationship with the feed channel design. Although assumptions (i) and (iii) are valid assumptions for a first initial comparison under laboratory conditions, they will become an important issue in the real application where real river and seawater are used.

4.4 Process and stack design

The final performance of the stack depends on a variety of parameters: (1) membrane properties (conductivity, selectivity, osmotic behavior), (2) cell properties (compartment thickness, spacer type), (3) stack design parameters (way of feed, electrodes), (4) operating conditions (flow rate, electrical load), and (5) water quality (salt content, impurities, temperature, composition). These different parameters often conflict with each other and all together they determine the final power output. Veerman et al. [6] systematically investigated the performance of a real RED stack with respect to power density and energy efficiency, especially focusing on the effect of the current density, the membrane and spacer resistance, and the feed flow rate. They used a custom-made RED stack with an adaptable number of cells, with a maximum of 50 cells (total effective membrane area of 1 m^2). Each cell consisted of an anion and a CEM with an effective membrane area of 100 cm^2 per membrane. Commercially available membranes from Fumasep (Germany) were used: FAD as AEM and FKD as CEM. These membranes have a thickness of 0.082 mm. Polyamide woven sheets with a thickness of 200 μm were used as spacer. As electrode system, the authors used a solution of 1 M NaCl with 0.05 M $K_4Fe(CN)_6$ and 0.05 M $K_3Fe(CN)_6$. Sea and river water were represented by NaCl solutions of, respectively, 30 and 1 g/L. The 50-cell stack generated a power output of 0.93 W, which is the highest power output reported for RED using sea and river water. Fig. 13 shows the power output of the stack as a function of the current density for different numbers of cells (N) [6].

The obtained power increases almost linearly with the number of cells, which indicates that the losses due to limiting currents are limited [36]. The maximum power obtainable in this stack is 0.93 W/m^2, which is the highest power reported in literature.

Not only the power output is an important parameter, the energy efficiency also plays a significant role. It represents the fraction of the total available energy available from the mixing of river and seawater that is really used to generate power. In the case of the stack experiments of Veerman et al. [6], the highest power density reported could be obtained. However, the energy efficiency at that point is no more than 50% [6]. So optimization with respect to obtained power only would result generally in low energy efficiencies and loss of potentially available energy. Post et al. [35] show that, in principle, no fundamental limitations restrict the energy efficient use of the resources and values as high as 80% can be obtained.

In the real application, the power density obtainable in a RED stack is often reduced due to parasitic currents, or also called current leakage in the

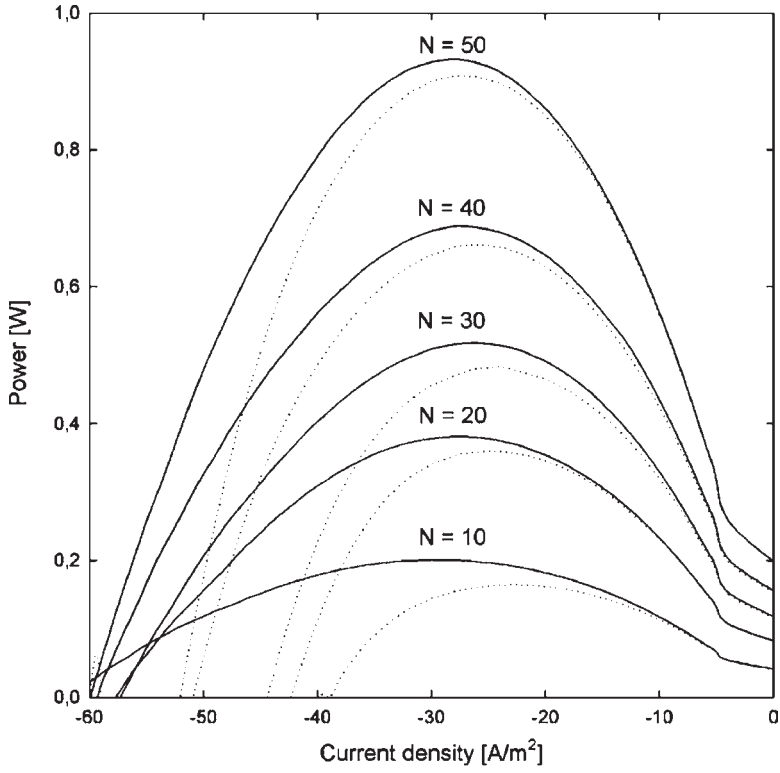

Figure 13 Experimentally determined power obtainable in RED when using sea and river water, as a function of the current density for different numbers of cells. The solid line represents the power generated by the stack and the dashed line is the output at the working electrodes [6].

stack. There are two sources of these losses [36]: (1) ion exchange membranes are never 100% selective, which apart from generating the transport of counterions, also generates a transport of co-ions, which reduces the power output. This issue is related to membrane design and optimization. (2) Ionic shortcut currents occur due to the transport of ions in feed and drain channels and this effect is more severe at higher salt concentrations. These ionic shortcut losses are strongly related to stack design.

In principle, three different ionic shortcut currents can be distinguished in the stack [36]:

1. Ionic shortcut currents in the electrode solution (the electrode solution connects the anode and the cathode compartment). These losses can be easily reduced by increasing the length of the tubing that connects the electrodes.

2. Ionic shortcut currents between the river water compartments. Generally, this shortcut current can be neglected because the salt concentration in the river water compartment is too low to cause significant leakages.
3. Shortcut currents between the seawater compartments.

Veerman et al. [36] investigated the possibilities to reduce the shortcut currents between the seawater compartments. Model calculations show that the effect of these losses can be significantly reduced through proper stack design. Especially important in this respect are the number of cells (N), the channel resistance in relation to the cell resistance (R/r), and the lateral spacer resistance in relation to the cell resistance (ρ/r), where the latter two are the critical design parameters that need to be optimized [36]. In medium-size stacks, the number of cells and the ratio R/r and $\rho/$r need to be as high as possible [36]. Possibilities to do so include (i) increasing the channel resistance (R) by narrowing the channels; (ii) increasing the lateral spacer resistance (ρ) by using thinner spacers (in the seawater compartment); and (iii) decreasing the cell resistance r by using membranes with low resistances and thin spacers (in the river water compartment). Possibilities to increase R are limited: with narrowing the channels, the hydrodynamical resistance in the channels also increases. An increase in the spacer resistance only induces a very small change in power output and the only way to increase the power output is to decrease the cell resistance, as it increases the efficiency and the power output of the system [36]. In very large stacks, (R/r) (the channel resistance in relation to the cell resistance) should be maximized to obtain the largest power output [36]. A decrease in r can be induced by minimization of the membrane thickness and the thickness of both the sea and the river water compartments, but this results in an equal decrease in the channel resistance, and consequently has no effect. But, at given membrane thickness and river water compartment dimensions, a decrease of the thickness of the seawater compartment induces a lower r and a higher R/r ratio and consequently a higher efficiency and power output [36].

4.5 Pilot testing and scale-up[2]

Wetsus – Center for Sustainable Water Technology in the Netherlands– started with the ''Blue Energy'' project in 2005 with a focus on RED. At that time, only a few scientific papers were published [4,28,31] about

[2]The information given in this paragraph section is provided by and property of the company REDstack B.V., The the Netherlands, and is used with permission. The authors would like to acknowledge REDstack B.V. for the contribution.

results of the RED system in a period of 50 years. Over the past few years, the performance of RED on laboratory scale has improved considerably. However, thus far, RED experiments have typically been performed on a small scale, varying from current-passing areas of just a few square centimeters [32] to hundreds of square centimeters [36] and from four cell-pairs [33] to fifty cell-pairs [38]. State-of-the-art is a stack with an active membrane area of $25 \times 75\,cm^2$ and 50 cell-pairs with a power output of about 16 W (Fig. 14; drawing prepared by REDstack B.V., the Netherlands, and belongs to the company; used with permission).

To achieve practical implementation, RED still needs to be scaled up by several orders of magnitude. This upscaling and practical implementation is beyond the academic expertise and needs to be done in close cooperation with industry. For this reason, REDstack B.V. was founded by Magneto Special Anodes B.V., the Netherlands and Landustrie/Hubert, two industrial companies participating within the Blue Energy research of Wetsus. The challenges still faced by REDstack B.V., concerning the economics, technological feasibility, and the developing path of RED, are the development of low-cost membranes, the pretreatment in relation to stack design and operation, and the upscaling.

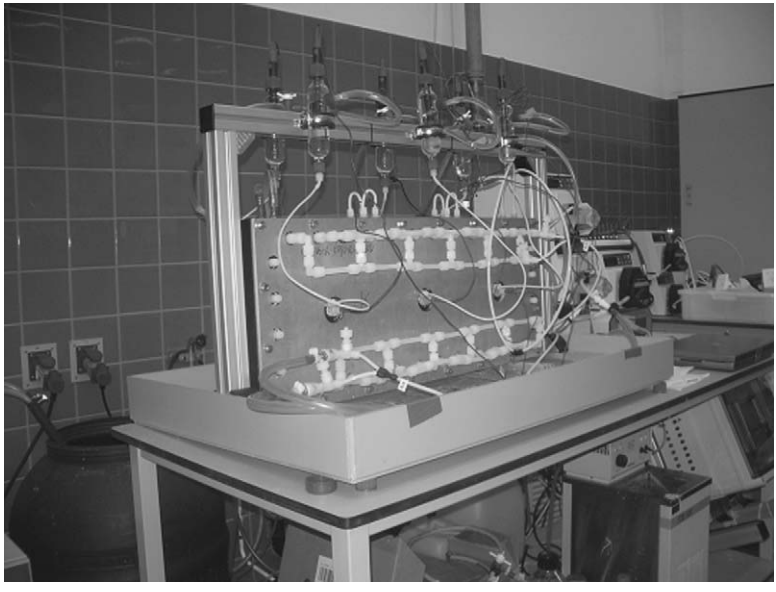

Figure 14 Reverse electrodialysis stack for research purposes with a total membrane area of $25 \times 75\,cm^2$ and 50 cell-pairs as manufactured by REDstack B.V., the Netherlands.

Although the technical requirements are already met by currently available membranes, the cost prices are out of range to make RED affordable. According to Turek and Bandura [32], it is hard to believe that the price of low-resistance ion exchange membranes may be reduced 100 times, which seems to be the desired cost level [32]. Nevertheless, for several reasons, REDstack B.V. is more optimistic that membrane prices for (reverse) electrodialysis can be reduced tremendously [31]. This is because of the fact that electrodialysis membranes have never had a considerable market share. Even then, on the global market, heterogeneous ion exchange membranes can be found with very low cost prices (<5 US\$/m^2). Of course, low-resistance ion exchange membranes command higher prices of 100 US\$/m^2 or more [32], but these prices can also be expected to fall, as manufacturing techniques improve, and the range of applications expands. Market research for related membrane applications show unit prices of installed membranes falling by an order of magnitude in 10 years, and this made Sutherland [54] to predict that the 1 US\$/m^2 of installed membrane is not far off. Second, it should be noticed that – apart from different technical requirements – the current membrane market would never be able to match the demand of required membrane area for power production. This implicates that besides the expertise in manufacturing of membranes the expertise of bulk production is also needed. While at the start of the membrane development, REDstack B.V. was dedicated to the technical requirements (as described previously) and cost prices of base materials, nowadays REDstack B.V. focuses on the scalability of the production process with focus on labor-extensive reel-to-reel production lines operating at high speeds.

Although addressed in scientific papers, challenges often not considered are the pretreatment of river water and seawater [34] and the hydrodynamic aspects of RED [55]. The required water quality parameters are still unknown. It is not likely to look at experiences in desalination stacks because the usually applied pretreatment steps [56] would be too capital-intensive to be viable for RED. Nevertheless, RED would require an extensive pretreatment as the distance between the membranes is less than in conventional flat-sheet membrane systems. It requires a more robust system design using the developed CFD model for flat-sheet membrane configurations [55]. Besides the cost aspect, also the footprint, energy consumption, and use of chemicals should be taken into account regarding the feasibility of RED.

The promising results raised the interest of different industrial and power supply companies and water authorities to invest in pilot tests. At this

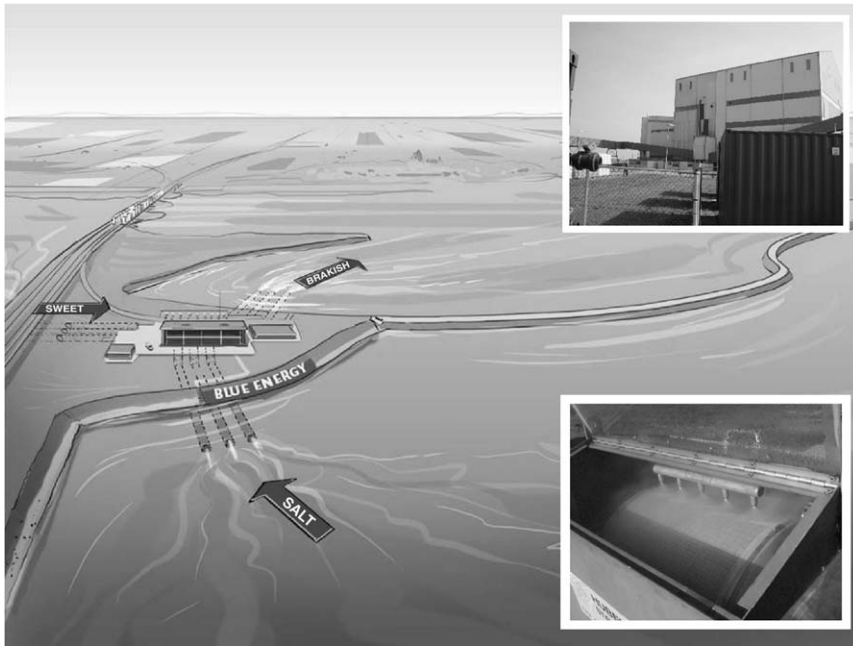

Figure 15 Artist impression of a salinity-gradient power plant at the IJsselmeer (by Rijkswaterstaat); inset top right: reverse electrodialysis pilot in Harlingen; inset bottom right: pretreatment pilot (REDstack B.V., The Netherlands).

stage of the project, focus is on consortium building, with customers entering into technical development agreements with suppliers, joint designs, and test programs. Parties agreed on the following development path for scale-up of the system (Fig. 15):

- Industrial pilot (kW-scale) on saline flows in a salt factory (financially supported by SenterNovem, Innowator project; 2008–2010).
- Feasibility study and definition of requirements for a communal power plant of 200 MW at the Afsluitdijk, The Netherlands (private funding, 2008).
- Communal pilot (10–40 kW) on seawater and river water (2009–2010) at the Afsluitdijk, The Netherlands.
- Communal demonstration plant (1 MW) on seawater and river water (2010–2012) at the Afsluitdijk, The Netherlands.

5. CONCLUDING REMARKS

This chapter clearly shows the huge potential of salinity gradient energy and the significant progress that has been made during recent years on both

PRO and RED. This has led to an increased power density for both technologies. Nevertheless, significant efforts are still required to make salinity gradient energy competitive with other new, renewable energy sources. For PRO, the reduction of external and internal concentration polarization is the main challenge, whereas for RED the main challenge is the reduction of the internal stack and membrane resistance. In addition, system design and pilot and demonstration plant testing using real feed waters are important issues to investigate. And, although not thoroughly investigated yet, but definitely important to consider is the positioning of such a system in the local environment without harming the ecological system, shipping traffic, and recreational activities.

REFERENCES

[1] O. Davidson, B. Metz, Special report on carbon dioxide capture and storage. Retrieved December 23, 2008, from Intergovernmental Panel on Climate Change Web site: http://www.ipcc.ch/pdf/special-reports/srccs/srccs_wholereport.pdf, 2005.
[2] G.L. Wick, W.R. Schmitt, Prospects for renewable energy from the sea, Marine Technol. Soc. J. 11(5 and 6) (1977) 16–21.
[3] J.W. Post, J. Veerman, H.V.M. Hamelers, G.J.W. Euverink, S.J. Metz, K. Nijmeijer, C.J.N. Buisman, Salinity-gradient power: evaluation of pressure-retarded osmosis and reverse electrodialysis, J. Membr. Sci. 288 (2007) 218–230.
[4] R.E. Pattle, Production of electric power by mixing fresh and salt water in the hydroelectric pile, Nature 174(4431) (1954) 660–661.
[5] H. Strathmann, Ion-exchange Membrane Separation Processes, 1st ed., Elsevier, Amsterdam, 2004.
[6] J. Veerman, M. Saakes, S.J. Metz, G.J. Harmsen, Reverse electrodialysis: performance of a stack with 50 cells o the mixing of sea, river water, J. Membr. Sci. 327 (2008) 136–144.
[7] S. Loeb, Production of energy from concentrated brines by pressure-retarded osmosis. 1. Preliminary technical and economic correlations, J. Membr. Sci. 1 (1976) 49–63.
[8] S. Loeb, F. Vanhessen, D. Shahaf, Production of energy from concentrated brines by pressure-retarded osmosis. 2. Experimental results and projected energy costs, J. Membr. Sci. 1 (1976) 249–269.
[9] S. Loeb, G.D. Mehta, 2-Coefficient water transport-equation for pressure retarded osmosis, J. Membr. Sci. 4 (1979) 351–362.
[10] S. Loeb, Energy production at the Dead Sea by pressure-retarded osmosis: challenge or chimera? Desalination 120 (1998) 247–262.
[11] S. Loeb, L. Titelman, E. Korngold, J. Freiman, Effect of porous support fabric on osmosis through a Loeb-Sourirajan type asymmetric membrane, J. Membr. Sci. 129 (1997) 243–249.
[12] S. Loeb, Large-scale power production by pressure-retarded osmosis, using river water and sea water passing through spiral modules, Desalination 143 (2002) 115–122.
[13] G.D. Mehta, S. Loeb, Internal polarization in the porous substructure of a semipermeable membrane under pressure-retarded osmosis, J. Membr. Sci. 4 (1978) 261–265.
[14] G.D. Mehta, S. Loeb, Performance of permasep b-9 and b-10 membranes in various osmotic regions and at high osmotic pressures, J. Membr. Sci. 4 (1979) 335–349.

[15] G.D. Mehta, Further results on the performance of present-day osmotic membranes in various osmotic regions, J. Membr. Sci. 10 (1982) 3–19.
[16] K.L. Lee, R.W. Baker, H.K. Lonsdale, Membranes for power-generation by pressure-retarded osmosis, J. Membr. Sci. 8 (1981) 141–171.
[17] S.E. Skilhagen, J.E. Dugstad, R.J. Aaberg, Osmotic power – power production based on the osmotic pressure difference between waters with varying salt gradients, Desalination 220 (2008) 476–482.
[18] K. Gerstandt, K.-V. Peinemann, S.E. Skilhagen, T. Thorsen, T. Holt, Membrane processes in energy supply for an osmotic power plant, Desalination 224 (2008) 64–70.
[19] J.R. McCutcheon, M. Elimelech, Influence of membrane support layer hydrophobicity on water flux in osmotically driven membrane processes, J. Membr. Sci. 318 (2008) 458–466.
[20] T. Thorsen, T. Holt, The potential for power production from salinity gradients by pressure retarded osmosis, J. Memb. Sci. 335(1–2) (2009) 103–110.
[21] R.L. McGinnis, J.R. McCutcheon, M. Elimelech, A novel ammonia-carbon dioxide osmotic heat engine for power generation, J. Membr. Sci. 305 (2007) 13–19.
[22] J.R. McCutcheon, M. Elimelech, Modeling water flux in forward osmosis: implications for improved membrane design, AIChE J. 53 (2007) 1736–1744.
[23] R.L. McGinnis, M. Elimelech, Energy requirements of ammonia-carbon dioxide forward osmosis desalination, Desalination 207 (2007) 370–382.
[24] J.R. McCutcheon, M. Elimelech, Influence of concentrative and dilutive internal concentration polarization on flux behavior in forward osmosis, J. Membr. Sci. 284 (2006) 237–247.
[25] G.T. Gray, J.R. McCutcheon, M. Elimelech, Internal concentration polarization in forward osmosis: role of membrane orientation, Desalination 197 (2006) 1–8.
[26] T.Y. Cath, A.E. Childress, M. Elimelech, Forward osmosis: principles, applications, and recent developments, J. Membr. Sci. 281 (2006) 70–87.
[27] E.R. Cornelissen, D. Harmsen, K.F. de Korte, C.J. Ruiken, J.J. Qin, H. Oo, L.P. Wessels, Membrane fouling and process performance of forward osmosis membranes on activated sludge, J. Membr. Sci. 319 (2008) 158–168.
[28] J.N. Wienstein, F.B. Leitz, Electric power from differences in salinity: the dialytic battery, Science 191 (1976) 557–559.
[29] R.E. Lacey, Energy by reverse electrodialysis, Ocean Eng. 7 (1980) 1–47.
[30] R. Audinos, Electrodialyse inverse. Etude de l'énergie électrique obtenue à partir de deux solutions de salinités differentes, J. Power Sources 10 (1983) 203–217.
[31] J. Jagur-Grodzinski, R. Kramer, Novel process for direct conversion of free energy of mixing into electric power, Ind. Eng. Chem. Process Des. Dev. 25 (1986) 443–449.
[32] M. Turek, B. Bandura, Renewable energy by reverse electrodialysis, Desalination 205 (2007) 67–74.
[33] M. Turek, B. Bandura, P. Dydo, Power production from coal-mine brine utilizing reversed electrodialysis, Desalination 221 (2008) 462–466.
[34] P. Długołęçki, K. Nijmeijer, S. Metz, M. Wessling, Current status of ion exchange membranes for power generation from salinity gradients, J. Membr. Sci. 319(1–2) (2007) 214–222.
[35] J.W. Post, H.V.M. Hamelers, C.J.N. Buisman, Energy recovery from controlled mixing salt and fresh water with a reverse electrodialysis system, Environ. Sci. Technol. 42(15) (2008) 5785–5790.
[36] J. Veerman, J.W. Post, M. Saakes, S.J. Metz, G.J. Harmsen, Reducing power losses caused by ionic shortcut currents in reverse electrodialysis stacks by a validated model, J. Membr. Sci. 310 (2008) 418–430.
[37] J. Veerman, M. Saakes, S.J. Metz, G.J. Harmsen, Reverse electrodialysis: performance of a stack with 50 cells on the mixing of sea and river water, J. Memb. Sci. 327(1–2) (2009) 136–144.

[38] F. Suda, T. Matsuo, D. Ushioda, Transient changes in the power output from the concentration difference cell (dialytic battery) between seawater and river water, Energy 32 (2007) 165–173.
[39] E. Brauns, Towards a world sustainable and simultaneous large-scale production of renewable energy and potable water through salinity gradient power by combining reversed electrodialysis and solar power? Desalination 219 (2008) 312–323.
[40] X. Tongwen, Y. Weihua, Fundamental studies of a new series of anion exchange membranes: membrane preparation and characterization, J. Membr. Sci. 190 (2001) 159–166.
[41] F.G. Wilhelm, I.G.M. Punt, N.F.A. van der Vegt, H. Strathmann, M. Wessling, Cation permeable membranes from blends of sulfonated poly (ether ether ketone) and poly (ether sulfone), J. Membr. Sci. 199 (2002) 167–176.
[42] P. Xing, G.P. Robertson, M.D. Guiver, S.D. Mikhailenko, K. Wang, S. Kaliaguine, Synthesis and characterization of sulfonated poly (ether ether ketone) for proton exchange membranes, J. Membr. Sci. 229 (2004) 95–106.
[43] R.K. Nagarale, G.S. Gohil, V.K. Shahi, R. Rangarajan, Preparation and electrochemical characterizations of cation-exchange membranes with different functional groups, Colloids Surf. A 251 (2004) 133–140.
[44] J. Schauer, L. Brozova, Z. Pientka, K. Bouzek, Heterogeneous ion-exchange polyethylene-based membranes with sulfonated poly(1,4-phenylene sulfide) particles, Desalination 200 (2006) 632–633.
[45] G.E. Molau, Heterogeneous ion-exchange membranes, J. Membr. Sci. 8 (1981) 309–330.
[46] F. Helfferich, Ion Exchange, McGraw Hill, New York, 1962.
[47] S. Koter, Influence of the layer fixed charge distribution on the performance of an ion-exchange membrane, J. Membr. Sci. 108 (1995) 177–183.
[48] Ralex, Ion exchange membranes, Product brochure Mega, a.s., Czech Republic.
[49] Selemion, Ion exchange membranes, Product brochure Asahi Glass Co., Ltd., Japan.
[50] Neosepta, Ion exchange membranes, Product brochure Tokuyama Co., Japan.
[51] Fumasep, Ion exchange membranes, Product brochure, FuMA-Tech GmbH, Germany.
[52] Y. Mizutani, Structure of ion exchange membranes, J. Membr. Sci. 49 (1990) 121–144.
[53] P.V. Vyas, B.G. Shah, G.S. Trivedi, P. Ray, S.K. Adhikary, R. Rangarajan, Characterization of heterogeneous anion-exchange membrane, J. Membr. Sci. 187 (2001) 39–46.
[54] K. Sutherland, Profile of the International Membrane Industry: Market Prospects to 2008, Elsevier, Amsterdam, 2003.
[55] M.H. Dirkse, W.P.K. van Loon, J.D. Stigter, J.W. Post, J. Veerman, G.P.A. Bot, Extending potential flow modelling of flat-sheet geometries as applied in membrane-based systems, J. Membr. Sci. 325 (2008) 537–545.
[56] J.P. Van der Hoek, D.O. Rijnbende, C.J.O. Lokin, P.A.C. Bonné, M.T. Loonen, M.H. Hofman, Electrodialysis as an alternative for reverse osmosis in an integrated membrane system, Desalination 117 (1998) 159–172.